

Phase Stability of Li-rich Layered Cathodes: Insight into the Debate over Solid Solutions vs Phase Separation

Zhi Lu, Shiqiang Hao, Ziliang Wang, Hyungjun Kim, and Christopher Wolverton*



Cite This: *Chem. Mater.* 2024, 36, 6381–6391



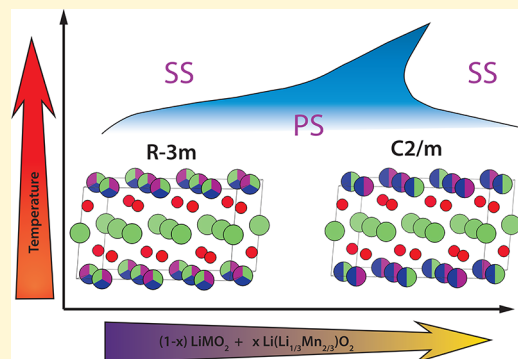
Read Online

ACCESS |

Metrics & More

Article Recommendations

ABSTRACT: Li-rich layered transition metal oxides ($\text{Li}_{1+x}\text{M}_{1-x}\text{O}_2$ or $m\text{Li}_2\text{MnO}_3-n\text{LiMO}_2$) have been widely studied as cathode materials for Li-ion batteries recently due to their enhanced capacity of larger than 250 mAh g⁻¹. However, even the qualitative nature of the phase stability of these materials, whether they form a solid solution or are phase separated, has been the subject of intense debate. In this work, we use density functional theory calculations to investigate the phase stability of these Li-rich layered transition metal oxides ($\text{Li}_2\text{MnO}_3-\text{LiMO}_2$, M = Co, Ni, Mn). We calculate the mixing enthalpy and coherency strain energy between Li_2MnO_3 and LiMO_2 for two distinct cases: (1) mixing of M on the Li and Mn sites respectively in the transition metal layer of Li_2MnO_3 , resulting in a solid solution with C2/m symmetry, and (2) mixing of Li and Mn on the M sites of LiMO_2 , resulting in a solid solution with R̄3m symmetry. We show that phase separation is energetically preferred relative to a solid solution at T = 0 K, and the coherency strain energy has little influence on phase stability. Results also display that a solid solution with R̄3m symmetry has a larger mixing enthalpy than that with C2/m symmetry at T = 0 K. Furthermore, we use the mixing enthalpies along with mean-field mixing entropies to calculate free energies and phase diagrams. At low temperature, the system exhibits phase separation between the C2/m and R̄3m phases, with appreciable solubility in each phase, and at high temperature, there is a transformation to the single-phase R̄3m solid solution. For high Li content compositions, the phase diagram shows a region of stability for the single phase C2/m solid solution. Our calculations support one possible explanation for the discrepancies between various reports of the structure of these Li-rich layered materials; the compositions and temperatures of these synthesized materials could be close to phase boundaries separating the regions of solid solution vs phase-separation. The calculated phase diagrams also indicate that the phase stability of Li-rich layered materials largely depends on the synthesis temperature, the amount of excess Li, and the combination of transition metals.



I. INTRODUCTION

Layered transition metal oxides (LiMO_2 , where M is usually Co, Mn, Ni, or their combination) have been widely studied and used as cathode materials for Li-ion batteries in the last four decades, since Goodenough showed that an open-circuit voltage versus Li of 4.0 V could be achieved using layered LiCoO_2 as the cathode material in 1980.^{1,2} However, these cathodes are limited in energy density, as they could only deliver reversible capacity from about 140 to 190 mAh g⁻¹.^{3,4} In the 1990s, the Thackeray^{5–10} and Dahn^{11–14} groups showed that the energy density could be increased by introducing excess Li in the transition metal layer, forming Li-rich layered transition metal oxides, $\text{Li}[\text{Li}_x\text{M}_{1-x}\text{O}_2]$.

Although these Li-rich layered transition metal oxides were introduced over two decades ago and have attracted much attention as cathode materials in Li-ion batteries because of their high capacity (larger than 250 mAh g⁻¹),^{8,15,16} there are still some uncertainty and severe challenges in these materials, including structural discrepancy,^{17–19} redox reaction mechanisms,^{20–25} poor rate performance,^{26–28} and voltage fade with

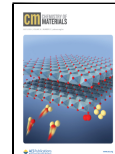
cycling.^{29–31} Due to the importance of the relationship between structure and the electrochemical properties of cathode materials, extensive experiments have been performed to unveil the structure of Li-rich cathode materials to understand their exceptional electrochemical performance,^{17–19,32–61} but the structure of the pristine material remains under debate. Studies that focused on solving the crystal structure of the pristine material have led to two conclusions. Some researchers proposed that these Li-rich layered $\text{Li}[\text{Li}_x\text{M}_{1-x}\text{O}_2]$ were composed of two phases, namely, the trigonal LiMO_2 structure (space group: R̄3m) and the monoclinic Li_2MnO_3 structure (space group: c2/m).^{7–10,19,42–53} On the other hand, some

Received: December 15, 2023

Revised: May 20, 2024

Accepted: May 21, 2024

Published: June 18, 2024



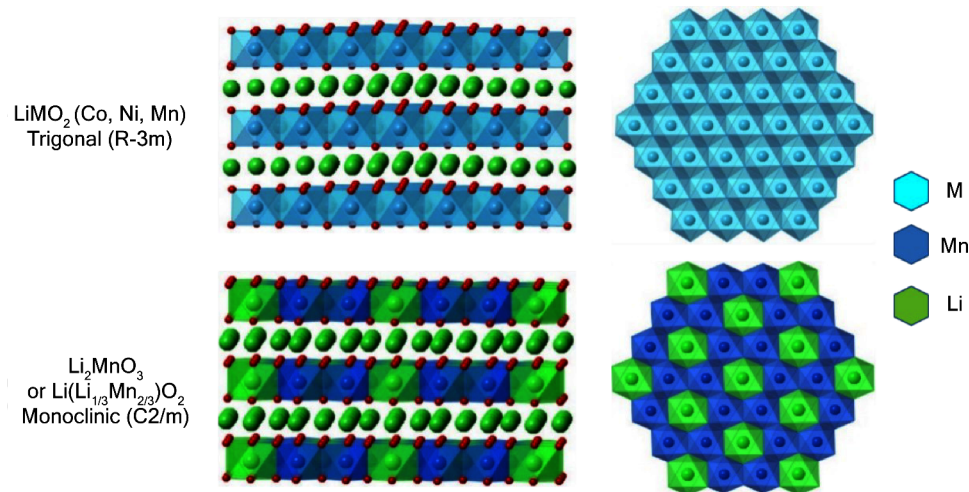
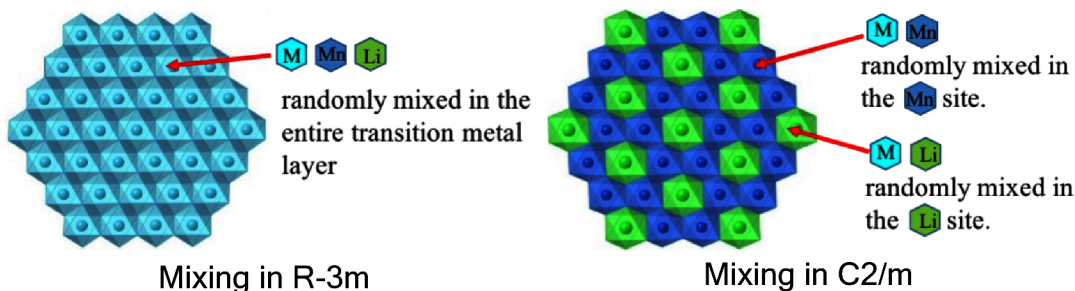


Figure 1. Structure of layered LiMO_2 ($M = \text{Mn, Ni, and Co}$) and Li_2MnO_3 and the corresponding transition metal layers. The main structural difference between LiMO_2 and Li_2MnO_3 is the cation ordering in the TM layer. In the TM layer in Li_2MnO_3 , one Li atom is surrounded by six Mn atoms, forming a cation ordered honeycomb type structure.



	TM Layer	Li Layer	Cation Ordering in TM Layer
LiMO_2	entire layer M	only Li	No
$\text{Li}(\text{Li}_{1/3}\text{Mn}_{2/3})\text{O}_2$	1/3 Li sites 2/3 Mn sites	only Li	Yes
R-3m solid solution	entire layer: Li, Mn and M mixing	only Li	No
C2/m solid solution	Li sites: Li and M mixing Mn sites: Mn and M mixing	only Li	Yes

Figure 2. Illustration of the solid solution model between $\text{Li}(\text{Li}_{1/3}\text{Mn}_{2/3})\text{O}_2$ and LiMO_2 in monoclinic $C2/m$ and trigonal $R\bar{3}m$ symmetry. The table summarizes the atomic configuration in the TM layered in both types of solid solution structures.

researchers argued that these two components formed a solid solution with $R\bar{3}m$ trigonal symmetry^{54–56} or $C2/m$ monoclinic symmetry.^{17,18,57–61}

In this paper, we aim to clarify the aforementioned structural controversy by investigating the phase stability of three systems, Li_2MnO_3 – LiMO_2 ($M = \text{Co, Ni, and Mn}$). We use first-principles calculations and special quasi-random structures (SQS) to study the competition between phase separation and solid solution formation.^{62–64} We first give a brief review of the structural complexity of these Li-rich layered transition metal oxides and the discrepancy in their phase stability. Following that, we introduce our atomic computational method to study and understand the structure of these Li-rich layered materials. Although extensive computational studies on the individual phases (trigonal phase^{65–68} and monoclinic phase^{69–73}) have

been conducted in the literature, very few attempts have been performed on the simulations of Li-rich layered compounds.^{74,75}

To understand whether the system Li_2MnO_3 – LiMO_2 favors phase separation or solid solution formation, we first generate the solid solution structures at several different compositions for each system using the SQS method and calculate mixing enthalpies of these solid solution structures in both trigonal $R\bar{3}m$ and monoclinic $C2/m$ systems. We also investigate the effect of coherency strain on the phase stability by calculating the strain energy. Calculation results show that thermodynamically phase separation is more favorable than solid solution at 0 K even when coherency strain energy is taken into account. Furthermore, we model the Gibbs free energies by fitting subregular solution models⁷⁶ and calculate the phase diagram for each system. The calculated phase diagram indicates that whether the system is

solid solution or phase separation depends largely on the synthesis temperature, the amount of excess Li, and the combination of transition metals. This work could help to understand the structural discrepancy and further investigate the influence of transition metal composition, Li content, and synthesis temperature on the structures of the Li-rich layered cathodes.

II. STRUCTURAL CONTROVERSY ON LI-RICH LAYERED CATHODES

II.A. Structures of LiMO_2 , Li_2MnO_3 , and Solid Solutions.

To review the structural controversy of these Li_2MnO_3 – LiMO_2 systems, we will first discuss the structure of the two parent phases, respectively. Layered LiMO_2 ($M = \text{Mn}, \text{Ni}, \text{Co}$) can be viewed as $\alpha\text{-NaFeO}_2$ -type rock salt structures with a transition metal (TM) layer and Li layer alternatively arranged in the O3 oxygen framework along the close packed direction. It often crystallizes in a trigonal system with $R\bar{3}m$ space group. In some of the literature, LiMO_2 is also categorized as hexagonal according to the crystal family or rhombohedral according to the lattice system. Different terminology could be used for this $R\bar{3}m$ phase. This work will use the trigonal phase to define layered LiMO_2 . The other component, Li_2MnO_3 , can be categorized as monoclinic with a $C2/m$ space group. This monoclinic $C2/m$ Li_2MnO_3 structure is quite similar to the trigonal $R\bar{3}m$ LiMO_2 structure and can be viewed as $\text{Li}[\text{Li}_{1/3}\text{Mn}_{2/3}]_{\text{O}}_2$ with the transition metal layer consisting of a periodic sequence of one Li and two Mn atoms. In the TM layer in Li_2MnO_3 , one Li atom is surrounded by six Mn atoms, forming a cation ordered honeycomb type structure, as shown in Figure 1.

Due to the similarity of the trigonal $R\bar{3}m$ and monoclinic $C2/m$ phases, there are structural discrepancies in the literature so far on whether these Li-rich layered oxides form homogeneous solid solutions between Li_2MnO_3 and LiMO_2 ^{17,18,54–61} or favor phase separation.^{7–10,19,42–53} Further, the solid solution could form with $R\bar{3}m$ or $C2/m$ monoclinic symmetry. Both structures keep the O3 oxygen sublattice and therefore only differ in cation arrangement. For the trigonal $R\bar{3}m$ solid solution, Li and Mn atoms in the TM layer from $\text{Li}(\text{Li}_{1/3}\text{Mn}_{2/3})_{\text{O}}_2$ and M atoms from LiMO_2 are randomly mixed in the entire TM layer. Experimentally, no cation ordering in the TM layer could be recognized in the $R\bar{3}m$ solid solution. For the monoclinic $C2/m$ solid solution, Li atoms in the TM layer from $\text{Li}(\text{Li}_{1/3}\text{Mn}_{2/3})_{\text{O}}_2$ and M atoms from LiMO_2 are mixed on the “Li sites” in the TM layer, while Mn atoms in the TM layer from $\text{Li}(\text{Li}_{1/3}\text{Mn}_{2/3})_{\text{O}}_2$ and M atoms from LiMO_2 are mixed on the “Mn sites” in the TM layer (Figure 2). In this way, the structure could be viewed as a single phase in space group $C2/m$, same as $\text{Li}(\text{Li}_{1/3}\text{Mn}_{2/3})_{\text{O}}_2$. Experimentally, cation ordering in the TM layer could be recognized in the $C2/m$ solid solution.

II.B. Evidence of Phase Separation and Solid Solution.

Due to the importance of the relationship between structure and the electrochemical properties of cathode materials for Li-ion batteries, it is essential to get a clear picture of the actual structure of these Li-rich layered transition metal oxides in order to understand and control their electrochemical performance. To address this issue, extensive experiments have been performed to unveil the structure of Li-rich cathode materials.^{17–19,32–61} X-ray diffraction (XRD), electron diffraction (ED), neutron diffraction (ND), high-resolution transmission electron microscopy (HRTEM), high-angle annular dark-field scanning transmission electron microscopy (HAADF-STEM), diffraction scanning transmission electron microscopy

(D-STEM), electron energy-loss spectroscopy (EELS), and other techniques have been used on various Li-rich layered oxides by different research groups. However, results obtained with these techniques by different research groups have been interpreted differently.

Some early research suggested Li-rich layered oxides were homogeneous solid solutions between the two components Li_2MnO_3 and LiMO_2 , because their lattice parameters varied linearly with the composition of its end members, which indicated that these samples follow Vegard’s rule.^{54,58} However, some researchers proposed the distribution of small isolated domains, on the scale of a few nanometers, could also exhibit behavior following Vegard’s law and would therefore be indistinguishable from solid solutions by only considering lattice parameters.⁷⁵ XRD and ND are techniques typically used for phase identification. However, the XRD and ND patterns of Li-rich layered oxides could be fitted to both phase separation and solid solution models.^{52,56} From the XRD pattern, some groups concluded that several weak peaks between 21 and 25°, which could not be indexed to $R\bar{3}m$ symmetry, were consistent with the LiMn_6 cation ordering that occurs in the transition metal layers of Li_2MnO_3 ; they could be indexed to the monoclinic unit cell, $C2/m$, which characterized the structure as a Li_2MnO_3 domain within a LiMO_2 matrix.^{10,11,44} On the other hand, some believed that these peaks resulted from long-range Li ordering in the transition metal layer, which could be the evidence of a solid solution in the $C2/m$ system.^{17,55–57} Some researchers also claimed that the weakening of these peaks between 21 and 25° resulted from stacking faults and not necessarily from the loss of long-range ordering in the transition-metal layer.⁵⁷ ED results also led to different conclusions. Some researchers suggested the extra streaks and spots in ED patterns represent the domain of Li_2MnO_3 ,^{44,56} while others interpreted it as a stacking fault.³⁴ Even for some recent studies using advanced atomic resolution techniques, such as HRTEM and high-resolution STEM, to investigate atomic structure directly, different conclusions have been proposed.^{17–19} By using D-STEM, Jarvis¹⁷ claimed that their Li-rich layered oxides sample was composed of a solid solution with $C2/m$ monoclinic symmetry and multiple planar defects. By systematically observing the entire primary particles along multiple zone axes using HAADF-STEM, Shukla¹⁸ suggested their Li-rich layered oxides samples were consistently made up of a single solid solution phase in $C2/m$ symmetry. On the other hand, direct observations of two phase coexistence from the atomic level were also reported. Yu¹⁹ showed the direct observation of the intergrowth of the Li_2MnO_3 -like structure with a bulk LiMO_2 structure by HRTEM and annular bright-field (ABF) STEM. Similar direct phase separation observation was also reported by Boulineau.⁴⁹

The results from all of these research groups indicate that the experimental identification of phase stability in the Li-rich layered oxides is difficult and sometimes contradictory. Even the same experimental evidence from the same characterization technique can be interpreted differently. Moreover, the direct observations of two-phase coexistence and a single solid solution phase in the entire sample indicate that it is highly possible that samples synthesized under different conditions with various chemical compositions could result in different structures. Little experimental research has been performed to study phase behavior of the Li-rich layered materials influenced by the synthesis temperature, transition metal composition, and excess Li content.^{36–38}

Thus, aiming to clarify the structural discrepancy, atomic computational tools could be used to theoretically investigate the phase stability of Li-rich layer systems as a function of temperature and two components content. So far, very few computational works have been performed on the phase stability of Li-rich layered compound.^{74,75} Xu⁷⁴ specifically studied $\text{Li}_{14/12}\text{Ni}_{1/4}\text{Mn}_{7/12}\text{O}_2$ ($0.5\text{Li}[\text{Li}_{1/3}\text{Mn}_{2/3}]\text{O}_3$ and $0.5\text{Li-Ni}_{1/2}\text{Mn}_{1/2}\text{O}_2$) with first-principles calculations. By constructing a supercell with two excess Li atoms occupying two of the 12 TM sites in the TM layer, several structure models of $\text{Li}_{14/12}\text{Ni}_{3/12}\text{Mn}_{7/12}\text{O}_2$ with different Li–TM configurations were created, and the calculated total energies were compared. With the lowest-energy structure, a positive mixing enthalpy around 40 meV per formula was achieved by comparing with two reference states, $\text{Li}[\text{Li}_{1/3}\text{Mn}_{2/3}]\text{O}_3$ and $\text{LiNi}_{1/2}\text{Mn}_{1/2}\text{O}_2$. Even though the positive mixing energy indicated phase separation, Xu argued that the Li-rich layered system was likely able to overcome the positive mixing energy and form a solid solution at high synthesis heating temperature. Iddir⁷⁵ investigated the Li_2MnO_3 – LiCoO_2 system with first-principles calculations. Solubility of Li_2MnO_3 in LiCoO_2 was supported by calculating the formation energy of a dilute distribution of LiMn_2 complexes embedded in the TM layers of LiCoO_2 . Results displayed very small solubility even at a high temperature. The solubility analysis suggests that, at the synthesis temperature, thermodynamics favored phase separation of composites $x\text{Li}_2\text{MnO}_3 \cdot (1-x)\text{LiCoO}_2$. Iddir also indicated that solid solution or relatively small Li_2MnO_3 domain sizes in Li-rich layered systems may result from other factors, such as coherency strain, which perhaps blocked domain coarsening in these materials. In our work, rather than the investigation at one certain concentration or dilute concentration assumption, we use density functional theory to theoretically investigate the phase stability of three Li-rich layer systems, Li_2MnO_3 – LiMO_2 ($\text{M} = \text{Co, Ni, Mn}$), as a function of temperature and over the entire component concentration. Furthermore, coherency strain energy is also calculated to study its impact on phase stability.

III. COMPUTATIONAL METHODOLOGY

Density functional theory (DFT) calculations are performed using the Vienna *ab initio* simulation package (VASP) within the generalized gradient approximation of Perdew–Burke–Ernzerhof for the exchange-correlation functional with Projector Augmented Wave (PAW) potentials and Hubbard U (GGA+U). All the calculations are performed with a plane wave basis set as implemented in VASP. The formation energies are converged to approximately 2 meV/cation using a basis set energy cutoff of 520 eV and k-point mesh with 4,000 k-points per reciprocal atom. The Hubbard U parameters for Co, Mn, and Ni atoms are U–J = 3.3, 3.9, and 6.2 eV, respectively. Since the energy differences between ferrimagnetic and ferromagnetic are usually small (less than 0.005 eV/atom in our case), we use ferromagnetic spins for Co, Mn, and Ni ions with initial magnetic moments of 0, 5, and 5 μB , respectively.

To calculate mixing enthalpies of the disordered solid solution, Special Quasi-random Structures (SQSs)⁶² are utilized to model random solid solutions between Li_2MnO_3 and LiMO_2 in both trigonal and monoclinic symmetry. SQSs are finite ordered structures, with atoms placed on lattice sites in such a way as to simulate pair and multibody correlations of a perfectly random network, up to the first few shells around a given site. In this way, SQSs enable an accurate DFT treatment of solid solutions, without the tremendous computational cost of an

extremely large supercell. In this work, SQSs are generated using a Monte Carlo algorithm based code “MCSQS” in Alloy Theoretic Automated Toolkit (ATAT).⁶³ We aim to match the pair correlation functions (up to 10 Å) of the generated solid solution structures to the ideal disordered state correlation.

IV. RESULTS AND DISCUSSION

Phase stability of three Li-rich layered oxide systems, Li_2MnO_3 – LiMO_2 ($\text{M} = \text{Co, Ni, Mn}$), is systematically investigated through first-principles calculations with the help of SQSs modeling. The model of phase stability used here consists of four steps. (1) SQSs are generated to model the solid solution structure between LiMO_2 ($\text{M} = \text{Co, Ni, Mn}$) and Li_2MnO_3 in both trigonal $\bar{R}\bar{3}m$ and monoclinic $C2/m$ symmetry. (2) Mixing enthalpies of the solid solution models are calculated from formation energy calculations of the generated SQSs. (3) Phase diagrams as a function of temperature and cation composition are calculated by fitting a subregular solution model to the mixing enthalpies and adding the configurational entropy. (4) Finally, coherency strain energy calculations provide the evidence of their influence on phase stability.

IV.A. SQSs generation. In our study, SQS structures are generated between $\text{Li}(\text{Li}_{1/3}\text{Mn}_{2/3})\text{O}_2$ and LiMO_2 at three different compositions, $0.25\text{Li}(\text{Li}_{1/3}\text{Mn}_{2/3})\text{O}_2$ – 0.75LiMO_2 , $0.5\text{Li}(\text{Li}_{1/3}\text{Mn}_{2/3})\text{O}_2$ – 0.5LiMO_2 , and $0.75\text{Li}(\text{Li}_{1/3}\text{Mn}_{2/3})\text{O}_2$ – 0.25LiMO_2 . All of the atom mixing takes place in the transition metal layer, between $(\text{Li}_{1/3}\text{Mn}_{2/3})$ and M. Although $\text{Li}(\text{Li}_{1/3}\text{Mn}_{2/3})\text{O}_2$ and LiMO_2 have similar layered structures with close lattice parameters, they are in different space groups, monoclinic $C2/m$ and trigonal $\bar{R}\bar{3}m$, respectively. And experimentally, both $C2/m$ solid solution^{17,18,58–61} and $\bar{R}\bar{3}m$ solid solution^{54–59} were reported in the literature. Thus, we generate solid solution models in both trigonal and monoclinic symmetry. For the trigonal $\bar{R}\bar{3}m$ solid solution model, Li and Mn atoms from the TM layer in $\text{Li}(\text{Li}_{1/3}\text{Mn}_{2/3})\text{O}_2$ and M atoms from LiMO_2 are mixed in the entire TM layer. For the monoclinic $C2/m$ solid solution model, Li atoms from the TM layer in $\text{Li}(\text{Li}_{1/3}\text{Mn}_{2/3})\text{O}_2$ and $1/3$ M atoms from LiMO_2 are mixed on the “Li sites” in the TM layer, while Mn atoms from $\text{Li}(\text{Li}_{1/3}\text{Mn}_{2/3})\text{O}_2$ and $2/3$ M atoms from LiMO_2 are mixed on the “Mn sites” in the TM layer (Figure 2). In this way, the generated SQSs could be viewed as solid solution with $C2/m$ symmetry, the same as $\text{Li}(\text{Li}_{1/3}\text{Mn}_{2/3})\text{O}_2$. The same sets of solid solution structures are used for all three systems, Li_2MnO_3 – LiCoO_2 , Li_2MnO_3 – LiNiO_2 , and Li_2MnO_3 – LiMnO_2 . Beyond the solid solution structures between $\text{Li}(\text{Li}_{1/3}\text{Mn}_{2/3})\text{O}_2$ and LiMO_2 , the $\bar{R}\bar{3}m$ solid solution $\text{Li}(\text{Li}_{1/3}\text{Mn}_{2/3})\text{O}_2$ is also constructed with one-third Li and two-thirds Mn atoms randomly arranged in the TM layer. The $\bar{R}\bar{3}m$ solid solution $\text{Li}(\text{Li}_{1/3}\text{Mn}_{2/3})\text{O}_2$ will be used as the reference state when calculating the mixing enthalpy in $\bar{R}\bar{3}m$ mixing systems.

IV.B. Mixing Enthalpy Calculation. We begin by introducing two different mixing enthalpies corresponding to two different type of solid solution models, the $C2/m$ mixing enthalpy, $\Delta H_{\text{mix}}^{\text{C}2/\text{m}}(x)$, and the $\bar{R}\bar{3}m$ mixing enthalpy, $\Delta H_{\text{mix}}^{\text{R}\bar{3}m}(x)$, where x (between 0 and 1) is the mole fractions of $\text{Li}(\text{Li}_{1/3}\text{Mn}_{2/3})\text{O}_2$. The mixing enthalpy is obtained by calculating the formation enthalpies of the SQSs relative to the reference parent states. For the $C2/m$ mixing, the reference states are LiMO_2 and $C2/m$ $\text{Li}(\text{Li}_{1/3}\text{Mn}_{2/3})\text{O}_2$ (with cation ordering in TM layer). For the $\bar{R}\bar{3}m$ mixing, the reference states

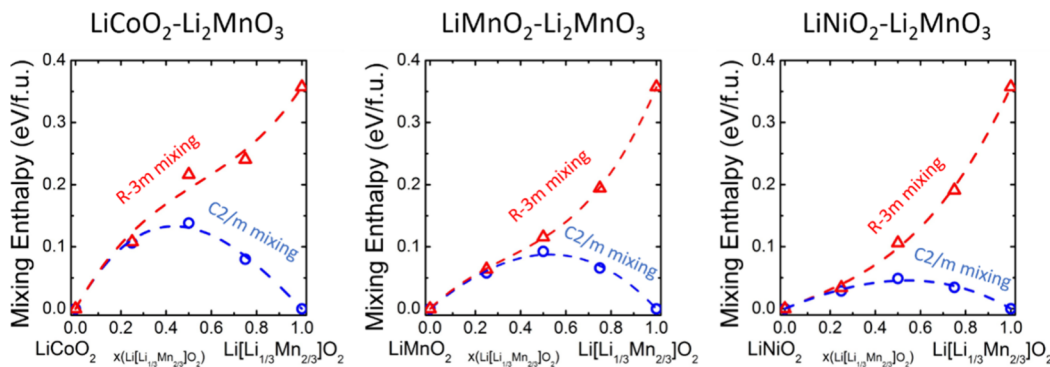


Figure 3. Mixing enthalpies between $\text{Li}(\text{Li}_{1/3}\text{Mn}_{2/3})\text{O}_2$ and LiMO_2 in both the $C2/m$ and $R\bar{3}m$ solid solution models (blue circles and red triangles). All of the solid solution structures give positive mixing enthalpies with respect to LiMO_2 and $C2/m$ $\text{Li}(\text{Li}_{1/3}\text{Mn}_{2/3})\text{O}_2$. And $R\bar{3}m$ solid solutions display larger mixing enthalpy than the corresponding $C2/m$ solid solutions. By fitting the subregular solution model, we achieve $C2/m$ solid solution mixing enthalpy curves (blue dashed line) and $R\bar{3}m$ solid solution mixing enthalpy curves (red dashed line) for three mixing systems.

are LiMO_2 and $R\bar{3}m$ solid solution $\text{Li}(\text{Li}_{1/3}\text{Mn}_{2/3})\text{O}_2$ (without cation ordering in the TM layer).

$$\Delta H_{\text{mix}}^{C2/m}(x) = E_{\text{SQS}}^{C2/m}(x) - xE_{\text{Li}(\text{Li}_{1/3}\text{Mn}_{2/3})\text{O}_2}^{C2/m} - (1-x)E_{\text{LiMO}_2}$$

$$\Delta H_{\text{mix}}^{R\bar{3}m}(x) = E_{\text{SQS}}^{R\bar{3}m}(x) - xE_{\text{Li}(\text{Li}_{1/3}\text{Mn}_{2/3})\text{O}_2}^{R\bar{3}m} - (1-x)E_{\text{LiMO}_2}$$

where $E_{\text{SQS}}^{C2/m}(x)$ and $E_{\text{SQS}}^{R\bar{3}m}(x)$ are the total energy of solid solution structures in $C2/m$ and $R\bar{3}m$ mixing systems, respectively. $E_{\text{Li}(\text{Li}_{1/3}\text{Mn}_{2/3})\text{O}_2}^{R\bar{3}m}$ is the total energy of solid solution $R\bar{3}m$ $\text{Li}(\text{Li}_{1/3}\text{Mn}_{2/3})\text{O}_2$ with 1/3 Li and 2/3 Mn atoms randomly arranged in the TM layer, while $E_{\text{Li}(\text{Li}_{1/3}\text{Mn}_{2/3})\text{O}_2}^{C2/m}$ is the total energy of ground state $C2/m$ $\text{Li}(\text{Li}_{1/3}\text{Mn}_{2/3})\text{O}_2$ with cation ordering in TM layer. Note that, for the two different $\text{Li}(\text{Li}_{1/3}\text{Mn}_{2/3})\text{O}_2$, the solid solution $R\bar{3}m$ phase has higher energy than the ground state $C2/m$ phase, around 0.36 eV/f.u., calculated by

$$\Delta E_{\text{Li}(\text{Li}_{1/3}\text{Mn}_{2/3})\text{O}_2}^{R\bar{3}m \vee C2/m} = E_{\text{Li}(\text{Li}_{1/3}\text{Mn}_{2/3})\text{O}_2}^{R\bar{3}m} - E_{\text{Li}(\text{Li}_{1/3}\text{Mn}_{2/3})\text{O}_2}^{C2/m}$$

Both the $C2/m$ and $R\bar{3}m$ mixing enthalpies of SQSs in each system are shown in Figure 3. We should note that the $R\bar{3}m$ mixing enthalpy shown in Figure 3 is the mixing enthalpy relative to ground state $C2/m$, in order to display the stability of both the $C2/m$ and $R\bar{3}m$ solid solution on the same graph.

Furthermore, to model the thermodynamics of solid–solid mixing of these systems in the whole range from $x = 0$ to $x = 1$, a subregular solution model,

$$\Delta H_{\text{mix}}^{C2/m}(x) = \alpha_{C2/m}x(1-x) + \beta_{C2/m}x(1-x)(1-2x)$$

$$\Delta H_{\text{mix}}^{R\bar{3}m}(x) = \alpha_{R\bar{3}m}x(1-x) + \beta_{R\bar{3}m}x(1-x)(1-2x)$$

$\Delta H_{\text{mix}}^{R\bar{3}m}(x) = \alpha_{R\bar{3}m}x(1-x) + \beta_{R\bar{3}m}x(1-x)(1-2x)$ is fit to the mixing enthalpies of three SQSs at $x = 0.25, 0.5$, and 0.75 with fitting parameters $\alpha_{C2/m}$ and $\beta_{C2/m}$ for the $C2/m$ solid solution model and $\alpha_{R\bar{3}m}$ and $\beta_{R\bar{3}m}$ for the $R\bar{3}m$ solid solution model.

As Figure 3 shows, in all the three mixing systems, $\text{Li}(\text{Li}_{1/3}\text{Mn}_{2/3})\text{O}_2$ – LiMO_2 ($M = \text{Co}, \text{Mn}, \text{Ni}$), both $C2/m$ and $R\bar{3}m$ mixing enthalpies are calculated at $x = 0.25, 0.5, 0.75$. All of the mixing enthalpies are positive with respect to LiMO_2 and ordered $C2/m$ $\text{Li}(\text{Li}_{1/3}\text{Mn}_{2/3})\text{O}_2$. That means it is more

energetically favorable to be phase separated at 0 K in $\text{Li}(\text{Li}_{1/3}\text{Mn}_{2/3})\text{O}_2$ – LiMO_2 systems. Also, $R\bar{3}m$ mixing displays higher energy than $C2/m$ mixing in all the systems. Furthermore, among these three systems, the LiNiO_2 – Li_2MnO_3 system shows the lowest mixing enthalpy around 40 meV per formula, which indicates Li-rich layered systems containing a large amount of Ni are more likely to overcome that small positive mixing energy and form solid solution at high synthesis temperature.

IV.C. Phase Diagram Calculation. To calculate phase diagram between $C2/m$ $\text{Li}(\text{Li}_{1/3}\text{Mn}_{2/3})\text{O}_2$ and $R\bar{3}m$ LiMO_2 , we first define two different Gibbs free energies of mixing, the $C2/m$ free energy of mixing, $\Delta G_{\text{mix}}^{C2/m}$, and the $R\bar{3}m$ free energy of mixing, $\Delta G_{\text{mix}}^{R\bar{3}m}$. Both free energies of mixing are functions of composition, x , and temperature, T .

$$\Delta G_{\text{mix}}^{C2/m}(x, T) = \Delta H_{\text{mix}}^{C2/m}(x) - T\Delta S_{\text{mix}}^{C2/m}(x)$$

$$\Delta G_{\text{mix}}^{R\bar{3}m}(x, T) = \Delta H_{\text{mix}}^{R\bar{3}m \vee C2/m}(x) - T\Delta S_{\text{mix}}^{R\bar{3}m}(x)$$

where ΔH is mixing enthalpies and ΔS is mean-field configurational entropy. Note that in our free energy model only the configurational entropy is taken into account. For the $C2/m$ mixing, it is the binary mixing of M–Li and M–Mn. ΔS could be expressed as

$$\Delta S_{\text{mix}}^{C2/m}(x) = -k_{\text{B}}[x \ln x + (1-x) \ln(1-x)]$$

$$\Delta S_{\text{mix}}^{C2/m}(x) = -k_{\text{B}}[x \ln x + (1-x) \ln(1-x)]$$

For the $R\bar{3}m$ mixing, the ternary mixing of M–Li–Mn could be expressed as

$$\Delta S_{\text{mix}}^{R\bar{3}m}(x) = -k_{\text{B}}\left[\frac{x}{3} \ln \frac{x}{3} + \frac{2x}{3} \ln \frac{2x}{3} + (1-x) \ln(1-x)\right]$$

Now the $C2/m$ and $R\bar{3}m$ Gibbs free energies of mixing for each system could be described as

$$\Delta G_{\text{mix}}^{C2/m}(x, T) = \alpha_{C2/m}x(1-x) + \beta_{C2/m}x(1-x)(1-2x) + Tk_{\text{B}}[x \ln x + (1-x) \ln(1-x)]$$

$$\Delta G_{\text{mix}}^{R\bar{3}m}(x, T) = \alpha_{R\bar{3}m}x(1-x) + \beta_{R\bar{3}m}x(1-x)(1-2x)$$

$$+ [E_{\text{Li}(\text{Li}_{1/3}\text{Mn}_{2/3})\text{O}_2}^{R\bar{3}m} - E_{\text{Li}(\text{Li}_{1/3}\text{Mn}_{2/3})\text{O}_2}^{C2/m}]x$$

$$+ Tk_{\text{B}}\left[\frac{x}{3} \ln \frac{x}{3} + \frac{2x}{3} \ln \frac{2x}{3} + (1-x) \ln(1-x)\right]$$

where $\alpha_{C2/m}$, $\beta_{C2/m}$, $\alpha_{R\bar{3}m}$, and $\beta_{R\bar{3}m}$ are calculated parameters.

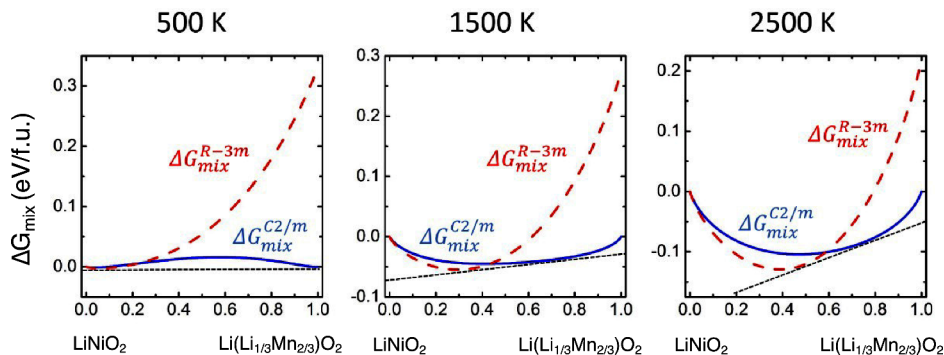


Figure 4. Illustration of $C2/m$ (blue solid line) and $R\bar{3}m$ (red dashed line) Gibbs free energies of mixing for the system $\text{LiNiO}_2-\text{Li}(\text{Li}_{1/3}\text{Mn}_{2/3})\text{O}_2$ as a function of mole fraction $\text{Li}(\text{Li}_{1/3}\text{Mn}_{2/3})\text{O}_2$ at $T = 500, 1500$, and 2500 K. The common tangent rule (dotted black line) shows the equilibrium concentrations of $\text{Li}(\text{Li}_{1/3}\text{Mn}_{2/3})\text{O}_2$ in the $C2/m$ and $R\bar{3}m$ phases. The intercepts of the tangent line with $x(\text{Li}(\text{Li}_{1/3}\text{Mn}_{2/3})\text{O}_2) = 0$ and 1 give the chemical potentials of LiNiO_2 and $\text{Li}(\text{Li}_{1/3}\text{Mn}_{2/3})\text{O}_2$, respectively.

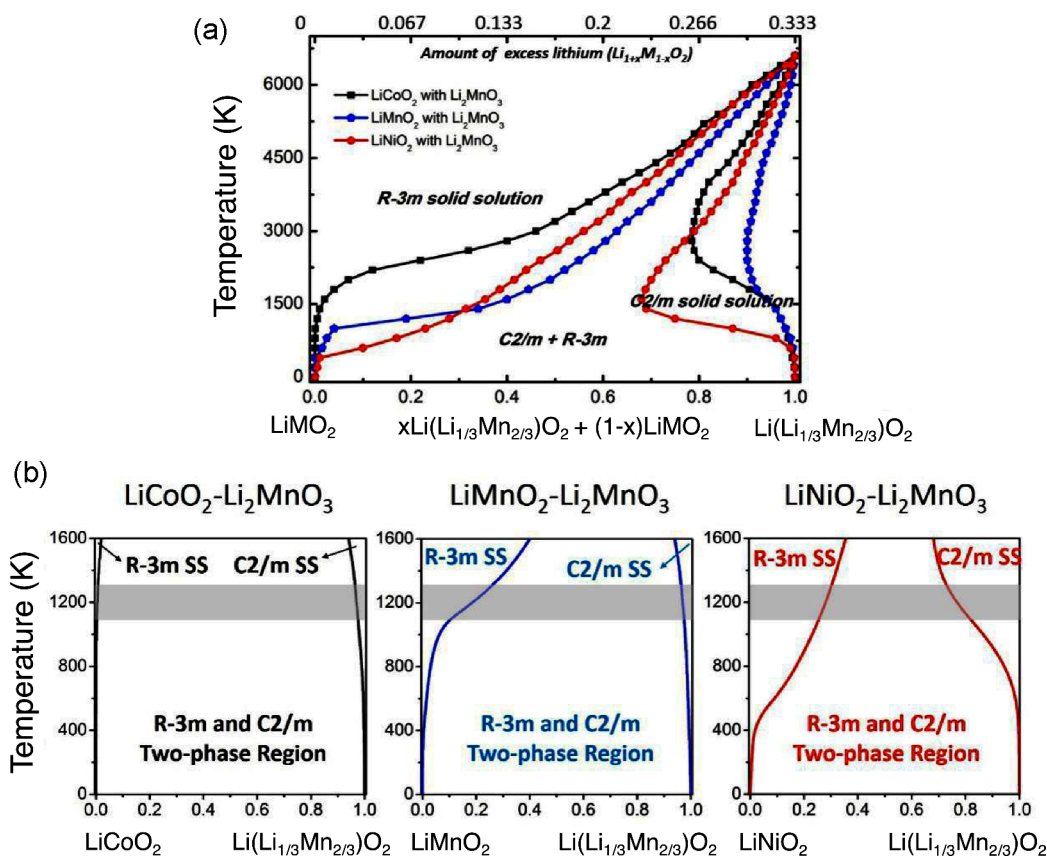


Figure 5. (a) Calculated phase diagram for $\text{Li}_2\text{MnO}_3-\text{LiMO}_2$ ($\text{M} = \text{Co}, \text{Mn}, \text{Ni}$) systems. The phase diagrams exhibit three phase regions, the $R\bar{3}m$ solid solution region, the $C2/m$ and $R\bar{3}m$ two-phase region and the $C2/m$ solid solution region. (b) Low temperature phase diagrams (<1600 K) for three $\text{Li}_2\text{MnO}_3-\text{LiMO}_2$ ($\text{M} = \text{Co}, \text{Mn}, \text{Ni}$) systems, respectively. The gray area on the phase diagram is the typical synthesis temperature range for Li-rich layered cathodes (1100–1300 K).

To illustrate the procedure of phase diagram calculation, we take the $\text{LiNiO}_2-\text{Li}(\text{Li}_{1/3}\text{Mn}_{2/3})\text{O}_2$ system as an example. The $C2/m$ and $R\bar{3}m$ Gibbs free energies of mixing for the $\text{LiNiO}_2-\text{Li}(\text{Li}_{1/3}\text{Mn}_{2/3})\text{O}_2$ system are illustrated in Figure 4 for temperatures at 500, 1500, and 2500 K. At each temperature, equilibrium between the two phases is found by setting the chemical potentials of each compound in each phase equal to each other.

$$\mu_{\text{LiMnO}_2}^{R\bar{3}m} = \mu_{\text{LiMnO}_2}^{C2/m}, \quad \mu_{\text{Li}(\text{Li}_{1/3}\text{Mn}_{2/3})\text{O}_2}^{R\bar{3}m} = \mu_{\text{Li}(\text{Li}_{1/3}\text{Mn}_{2/3})\text{O}_2}^{C2/m}$$

This procedure is illustrated graphically in Figure 4 as a common-tangent rule. The chemical potentials of the compounds can be found from the Gibbs free energy ($C2/m$ and $R\bar{3}m$) via

$$\mu_{\text{LiMnO}_2}(x) = \Delta G_{\text{mix}}(x) - x \frac{\partial \Delta G_{\text{mix}}(x)}{\partial x}$$

$$\mu_{\text{Li}(\text{Li}_{1/3}\text{Mn}_{2/3})\text{O}_2}(x) = \Delta G_{\text{mix}}(x) + (1 - x) \frac{\partial \Delta G_{\text{mix}}(x)}{\partial x}$$

Table 1. Summarization of Some Li-Rich Layered Oxides Which Have Been Experimentally Synthesized, Including Their Compositions, Synthesis Temperatures, and Experimentally Observed Phase Stabilities^a

Compound formula	Composition $x\text{Li}[\text{Li}_{0.33}\text{Mn}_{0.67}]\text{O}_2 + (1-x)\text{LiMO}_2$	Temperature (K)	Phase stability	Ref
$\text{Li}_{1.07}\text{Mn}_{0.53}\text{Ni}_{0.4}\text{O}_2$	$0.2\text{Li}[\text{Li}_{0.33}\text{Mn}_{0.67}]\text{O}_2 + 0.8\text{LiMn}_{0.5}\text{Ni}_{0.5}\text{O}_2$	1173	$\bar{R}3m$ SS	59
$\text{Li}_{1.13}\text{Mn}_{0.57}\text{Ni}_{0.3}\text{O}_2$	$0.39\text{Li}[\text{Li}_{0.33}\text{Mn}_{0.67}]\text{O}_2 + 0.61\text{LiMn}_{0.5}\text{Ni}_{0.5}\text{O}_2$	1273, 1173	Two Phase	9, 59
$\text{Li}_{1.13}\text{Mn}_{0.464}\text{Ni}_{0.203}\text{Co}_{0.203}\text{O}_2$	$0.39\text{Li}[\text{Li}_{0.33}\text{Mn}_{0.67}]\text{O}_2 + 0.61\text{LiMn}_{0.33}\text{Ni}_{0.33}\text{Co}_{0.33}\text{O}_2$	1073–1273	Two Phase	43
$\text{Li}_{1.167}\text{Mn}_{0.5}\text{Ni}_{0.167}\text{Co}_{0.167}\text{O}_2$	$0.5\text{Li}[\text{Li}_{0.33}\text{Mn}_{0.67}]\text{O}_2 + 0.5\text{LiMn}_{0.33}\text{Ni}_{0.33}\text{Co}_{0.33}\text{O}_2$	1173	Two Phase	44
$\text{Li}_{1.2}\text{Mn}_{0.4}\text{Co}_{0.4}\text{O}_2$	$0.6\text{Li}[\text{Li}_{0.33}\text{Mn}_{0.67}]\text{O}_2 + 0.4\text{LiCoO}_2$	1173	Two Phase	46, 53
$\text{Li}_{1.2}\text{Mn}_{0.6}\text{Ni}_{0.2}\text{O}_2$	$0.6\text{Li}[\text{Li}_{0.33}\text{Mn}_{0.67}]\text{O}_2 + 0.4\text{LiMn}_{0.5}\text{Ni}_{0.5}\text{O}_2$	1173	Two Phase	50
$\text{Li}_{1.2}\text{Mn}_{0.525}\text{Ni}_{0.1}\text{Co}_{0.175}\text{O}_2$	$0.6\text{Li}[\text{Li}_{0.33}\text{Mn}_{0.67}]\text{O}_2 + 0.4\text{LiMn}_{0.3125}\text{Ni}_{0.25}\text{Co}_{0.4375}\text{O}_2$	1173	Two Phase	50
$\text{Li}_{1.2}\text{Mn}_{0.55}\text{Ni}_{0.15}\text{Co}_{0.1}\text{O}_2$	$0.6\text{Li}[\text{Li}_{0.33}\text{Mn}_{0.67}]\text{O}_2 + 0.4\text{LiMn}_{0.375}\text{Ni}_{0.375}\text{Co}_{0.25}\text{O}_2$	1173	Two Phase	52
$\text{Li}_{1.2}\text{Mn}_{0.567}\text{Ni}_{0.166}\text{Co}_{0.067}\text{O}_2$	$0.6\text{Li}[\text{Li}_{0.33}\text{Mn}_{0.67}]\text{O}_2 + 0.4\text{LiMn}_{0.42}\text{Ni}_{0.42}\text{Co}_{0.16}\text{O}_2$	1173, 1273	Two Phase	19, 51
$\text{Li}_{1.2}\text{Mn}_{0.6}\text{Ni}_{0.2}\text{O}_2$	$0.6\text{Li}[\text{Li}_{0.33}\text{Mn}_{0.67}]\text{O}_2 + 0.4\text{LiMn}_{0.5}\text{Ni}_{0.5}\text{O}_2$	1123, 1273, 1173	$C2/m$ SS	17, 58, 59
$\text{Li}_{1.2}\text{Mn}_{0.533}\text{Ni}_{0.133}\text{Co}_{0.133}\text{O}_2$	$0.6\text{Li}[\text{Li}_{0.33}\text{Mn}_{0.67}]\text{O}_2 + 0.4\text{LiMn}_{0.33}\text{Ni}_{0.33}\text{Co}_{0.33}\text{O}_2$	1173	$C2/m$ SS	18
$\text{Li}_{1.2}\text{Mn}_{0.55}\text{Ni}_{0.15}\text{Co}_{0.1}\text{O}_2$	$0.6\text{Li}[\text{Li}_{0.33}\text{Mn}_{0.67}]\text{O}_2 + 0.4\text{LiMn}_{0.375}\text{Ni}_{0.375}\text{Co}_{0.25}\text{O}_2$	1173	$C2/m$ SS	61

^aThe “solid solution vs. phase-separation” debates mainly come from the Li-rich layered oxides with a large amount of excess, of which the compositions and temperature could be close to phase boundaries separating the regions of $C2/m$ solid solution vs. phase-separation.

By calculating equilibrium concentrations at various temperatures based on the common-tangent rule, phase diagrams are constructed for each of the Li_2MnO_3 – LiMO_2 system (Figure 5a). As the calculated phase diagram shows, there are three phase regions, the single phase $\bar{R}3m$ solid solution region, the $C2/m$ and $\bar{R}3m$ two-phase region, and the single phase $C2/m$ solid solution region. We find that at low temperature the system exhibits phase separation between the $C2/m$ and $\bar{R}3m$ phases, with appreciable solubility in each phase, and at high temperature there is a transformation to the single-phase $\bar{R}3m$ solid solution. For high Li content compositions, the phase diagram shows a region of stability for the single phase $C2/m$ solid solution.

The calculated phase transition temperature for Li_2MnO_3 from ordered $C2/m$ to $\bar{R}3m$ solid solution is very high (~6700 K), a reflection of the competition between the DFT energy at 0 K which strongly favors $C2/m$ and the configurational entropy of mixing that favors the $\bar{R}3m$ phase at high temperature. At a certain temperature below 6700 K, Li_2MnO_3 should exhibit other phase transitions such as decomposition before it transforms to $\bar{R}3m$ solid solution Li_2MnO_3 . In our calculation, we do not consider these complicated phase transitions at that high temperature, since the typical synthesis temperature of Li-rich layered cathodes is 1100–1300 K and the phase stability in this temperature range is more important. To better illustrate the phase stability at synthesis temperature, we draw the phase diagram which only shows the low temperature part (<1600 K) for each system respectively in Figure 5b.

At the typical synthesis temperature, the $\bar{R}3m$ solid solution forms first when the $C2/m$ Li_2MnO_3 phase is gradually added to the $\bar{R}3m$ LiMO_2 phase. After crossing the phase boundary between the $\bar{R}3m$ solid solution single phase region and two-phase region, $C2/m$ and $\bar{R}3m$ phase separation occurs. When more $C2/m$ Li_2MnO_3 is added to the system, the phase stability eventually favors the $C2/m$ solid solution over phase separation. We should note the amount of $C2/m$ phase could also be viewed as the amount of excess Li in Li-rich layered systems. Thus, the phase transition from the single phase $\bar{R}3m$ solid solution to the $C2/m$ and $\bar{R}3m$ two phase separation, and further to the single phase $C2/m$ solid solution, is predicted as a function of excess Li content. Similar phase transition evidence has been reported experimentally by McCalla³⁶ and Jarvis.³⁸ They both suggested the phase transition from phase separation to $C2/m$ solid solution when the amount of excess Li increased. The calculated

phase diagrams also indicate that the Li-rich systems with different mixing transition metals (Co, Mn, and Ni) display different phase behaviors. At synthesis temperature, in the Li_2MnO_3 – LiNiO_2 system, the $\bar{R}3m$ and $C2/m$ two-phase region is much narrower than the other two systems. The Li_2MnO_3 – LiCoO_2 system shows much lower Li_2MnO_3 solubility in the $\bar{R}3m$ phase than the other two systems. In our model, the solubility of Li_2MnO_3 in LiCoO_2 at 1100 K is only 0.005, which is consistent with Iddir's dilute calculation,⁷⁵ finding that the solubility of Li_2MnO_3 in LiCoO_2 at 1100 K is 0.006.

To further compare the experimentally synthesized Li-rich layered oxides with our calculated phase diagram, we summarize some Li-rich layered compounds which have been experimentally studied in Table 1, including their compositions, synthesis temperatures, and experimentally observed phase stabilities. Some research groups showed that $\text{Li}_{1.2}\text{Mn}_{0.4}\text{Co}_{0.4}\text{O}_2$ ($0.6\text{Li}[\text{Li}_{0.33}\text{Mn}_{0.67}]\text{O}_2 + 0.4\text{LiCoO}_2$) exhibits phase separation between $C2/m$ $\text{Li}[\text{Li}_{0.33}\text{Mn}_{0.67}]\text{O}_2$ and $\bar{R}3m$ LiCoO_2 . This is consistent with our calculation since this compound is in the two-phase region on the $\text{Li}[\text{Li}_{0.33}\text{Mn}_{0.67}]\text{O}_2$ – LiCoO_2 phase diagram. For the other $\text{Li}[\text{Li}_{0.33}\text{Mn}_{0.67}]\text{O}_2$ – LiMO_2 systems, our calculations only consider M in LiMO_2 to be pure Mn, Ni, and Co to simplify the problem. However, as we could see from Table 1, experimentally M is usually the combination of Mn, Ni, and Co. The various combinations in the transition metal layer could lead to the shift of phase boundary on the phase diagram and we could not directly compare these experimental synthesized compounds with our phase diagram. From Table 1, we could see that the “solid solution vs phase-separation” debates mainly come from the Li-rich layered oxides with large amount of excess Li. For high Li content compositions, the calculated phase diagram shows a region of stability for the single phase $C2/m$ solid solution. This suggests one possible explanation for the structure discrepancies of Li-rich layered materials between various reports: that some of the compositions and temperatures of these synthesized materials could be close to phase boundaries separating the regions of $C2/m$ solid solution vs phase-separation.

The calculated phase diagram shows that the phase stability of the Li-rich layered materials should be influenced by the synthesis temperature, the amount of excess Li, and the combination of transition metals. The calculated phase diagram could not only help to understand why researchers have different findings about the structure of this kind of Li-rich layered

cathode but also give insight into designing cathodes with different structures (solid solution or phase separation) by varying transition metal composition, Li content, and synthesis temperature.

IV.D. Coherency Strain Energies. In this section, we study the coherency strain effect on phase stability in Li-rich layer Li_2MnO_3 – LiMO_2 . The coherency strain energy is the energy required to strain two phases onto the same lattice parameter along a crystallographic direction. If the coherency strain energy is large enough to be comparable with incoherency mixing enthalpies, coherent phase separation may not happen, even though incoherency mixing enthalpies are positive. In the Li_2MnO_3 – LiMO_2 ($M = \text{Co}, \text{Mn}, \text{Ni}$) system, the $C2/m$ monoclinic phase and $R\bar{3}m$ trigonal phase have similar layered structure with close lattice parameters. The relaxed lattice constants of each compound are listed in Table 2. Note that the

Table 2. Lattice Constants of $C2/m$ Li_2MnO_3 and $R\bar{3}m$ LiMO_2 ($M = \text{Co}, \text{Mn}, \text{Ni}$)

Lattice constants	Li_2MnO_3	LiCoO_2	LiMnO_2	LiNiO_2
a (Å)	5.00	4.92	5.51	5.04
b (Å)	8.65	8.52	8.59	8.56
c (Å)	5.09	5.00	5.42	5.08

lattice constants of the $R\bar{3}m$ trigonal phases in Table 2 are converted to the corresponding $C2/m$ monoclinic cell to better display the lattice difference. Lattice constants a and b are along two crystallographic directions in the close packed layer, and lattice constant c is along the crystallographic direction out of the close packed layer.

In Li-rich layer systems, evidence of both solid solutions and phase separation have been reported experimentally, as we discussed in Section II. For those who found the phase separation of Li-rich layer Li_2MnO_3 – LiMO_2 systems, the images their atomic resolution electron microscopy often display coherency phase separation. As a result, some

researchers proposed it might be the coherency strain energy preventing phase separation from solid solution or blocking further domain coarsening in these Li-rich layer systems. Thus, in this section, we use first-principles calculations to study the coherency strain effect on phase stability in Li-rich layer Li_2MnO_3 – LiMO_2 . A method for calculating the coherency strain energy is given below, following refs 64 and 77.

Coherency strain energy depends on the crystallographic direction, k , and the amount of each phase, x . Generally, at a certain composition, the lowest coherency strain energy among all different crystallographic directions is regarded as the effective coherency strain energy in phase separation. This minimum coherency strain energy could be achieved in three steps.

We start by calculating the energy required to strain one phase to certain lattice constants in the plane perpendicular to k , while lattice constant a_{\parallel} along k is allowed to relax to minimize energy. We define this required energy as epitaxial strain energy, and for each phase we have

$$\Delta E_{\text{LiMO}_2}(k, a_{\perp}) = \min_{a_{\parallel}} [E_{\text{LiMO}_2}(k, a_{\perp}, a_{\parallel}) - E_{\text{LiMO}_2}(a_0)]$$

$$\Delta E_{\text{Li}_2\text{MnO}_3}(k, a_{\perp}) = \min_{a_{\parallel}} [E_{\text{Li}_2\text{MnO}_3}(k, a_{\perp}, a_{\parallel}) - E_{\text{Li}_2\text{MnO}_3}(a_0)]$$

where $E_{\text{LiMO}_2}(a_0)$ and $E_{\text{Li}_2\text{MnO}_3}(a_0)$ are the energies of phases LiMO_2 and Li_2MnO_3 at their equilibrium lattice parameters. The coherency strain energy in a certain direction, $\Delta E_{\text{CS}}(k, x)$, could be calculated by straining both phases LiMO_2 and Li_2MnO_3 to the same lattice constant in the plane perpendicular to k , and then minimizing the total strain energy of the system with respect to this lattice constant a_{\perp} .

$$\Delta E_{\text{CS}}(k, x) = \min_{a_{\perp}} [(1-x)\Delta E_{\text{Li}_2\text{MnO}_3}(k, a_{\perp}) + x\Delta E_{\text{LiMO}_2}(k, a_{\perp})]$$

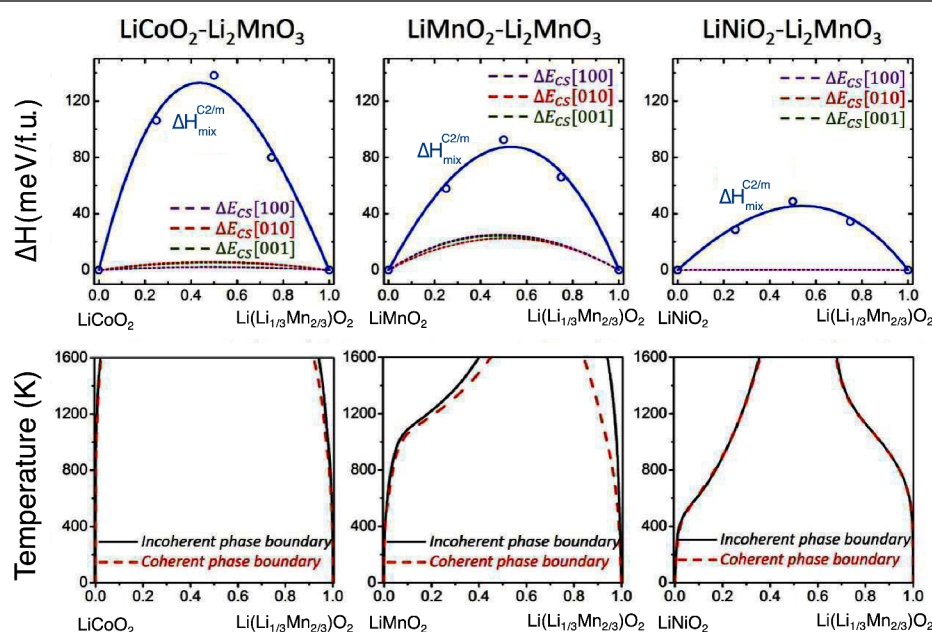


Figure 6. Coherency strain energy compared with incoherency mixing enthalpies and corresponding incoherent phase diagrams for each system. The coherency strain energies are much smaller compared with the incoherency mixing enthalpies, and the phase boundaries do not move significantly.

Furthermore, by varying the direction k , we could obtain the minimum coherency strain energy in the softest direction.

$$\Delta E_{CS}^{\min}(x) = \min_k [\Delta E_{CS}(k, x)]$$

In the Li_2MnO_3 – LiMO_2 systems, three directions [100], [010], and [001] within the $C2/m$ monoclinic cell are taken into account. [100] and [010] are in the close packed layer and [001] is out of the close packed layer. Figure 6 shows the coherency strain energy compared with incoherency $C2/m$ mixing enthalpies and the corresponding coherent phase diagram for each system.

In all three systems, the coherency strain energies are much smaller compared with the incoherency mixing enthalpies, and the phase boundaries in the coherent phase diagrams do not move significantly from the incoherent phase boundaries. This indicates that coherency strain is not a key factor to influence the phase stability in the Li-rich layered oxide systems.

V. CONCLUSION

To understand whether the Li-rich layered cathode materials phase separate or form solid solutions, the phase stabilities of three systems, Li_2MnO_3 – LiMO_2 ($M = \text{Co}, \text{Ni}, \text{Mn}$), are systematically investigated through first-principles calculations. By calculating the mixing enthalpy between Li_2MnO_3 and LiMO_2 and corresponding coherency strain energy, we show that, thermodynamically, phase separation is more favorable than solid solution at 0 K, and the coherency strain energy has little influence on phase stability. Also, $R\bar{3}m$ mixing displays higher energy than $C2/m$ mixing in all the systems at 0 K. The calculated phase diagrams indicate that the phase stability of Li-rich layered materials largely depends on the synthesis temperature, the amount of excess Li, and the combination of transition metals. At typical synthesis temperatures, phase transition from single phase $R\bar{3}m$ solid solution to the $C2/m$ and $R\bar{3}m$ two phase separation and further to the single phase $C2/m$ solid solution is predicted as a function of excess Li content. We find at low temperature the system exhibits phase separation between the $C2/m$ and $R\bar{3}m$ phases, with appreciable solubility in each phase, and at high temperature there is a transformation to the single-phase $R\bar{3}m$ solid solution. For high Li content compositions, the phase diagram shows a region of stability for the single phase $C2/m$ solid solution. Our calculation results suggest one possible explanation for the structural discrepancies of Li-rich layered materials between various reports is that the compositions and temperatures of these synthesized materials could be close to phase boundaries separating the regions of solid solution vs phase-separation.

■ AUTHOR INFORMATION

Corresponding Author

Christopher Wolverton – Department of Materials Science & Engineering, Northwestern University, Evanston, Illinois 60208, United States; orcid.org/0000-0003-2248-474X; Email: c-wolverton@northwestern.edu

Authors

Zhi Lu – Department of Materials Science & Engineering, Northwestern University, Evanston, Illinois 60208, United States
Shiqiang Hao – Department of Materials Science & Engineering, Northwestern University, Evanston, Illinois 60208, United States; orcid.org/0000-0002-7985-4468

Ziliang Wang – Department of Materials Science & Engineering, Northwestern University, Evanston, Illinois 60208, United States; orcid.org/0000-0002-6705-2329

Hyungjun Kim – Department of Materials Science & Engineering, Northwestern University, Evanston, Illinois 60208, United States; orcid.org/0000-0003-0879-0871

Complete contact information is available at:
<https://pubs.acs.org/10.1021/acs.chemmater.2c00927>

Notes

The authors declare no competing financial interest.

■ ACKNOWLEDGMENTS

ZL, SH, and CW acknowledge support from The Dow Chemical Company. ZW acknowledges support from Ford Motor Company, and HK acknowledges support from the Office of Naval Research, under Award N00014-23-1-2311. This research used resources of the National Energy Research Scientific Computing Center, a DOE Office of Science User Facility supported by the Office of Science of the U.S. Department of Energy, under Contract DE-AC02-05CH11231.

■ REFERENCES

- (1) Mizushima, K.; Jones, P. C.; Wiseman, P. J.; Goodenough, J. B. $\text{Li}_{1-x}\text{CoO}_2$ ($0 < x < 1$): A new cathode material for batteries of high energy density. *Mater. Res. Bull.* **1980**, *15*, 783.
- (2) Tarascon, J. M.; Armand, M. Issues and challenges facing rechargeable lithium batteries. *Nature* **2001**, *414*, 359–367.
- (3) Goodenough, J. B.; Park, K.-S. The Li-Ion Rechargeable Battery: A Perspective. *J. Am. Chem. Soc.* **2013**, *135*, 1167–1176.
- (4) Thackeray, M. M.; Wolverton, C.; Isaacs, E. D. Electrical energy storage for transportation—approaching the limits of, and going beyond, lithium-ion batteries. *Energy & Environ. Sci.* **2012**, *5*, 7854.
- (5) Rossouw, M.; Thackeray, M. Lithium manganese oxides from Li_2MnO_3 for rechargeable lithium battery applications. *Materials research bulletin* **1991**, *26*, 463.
- (6) Thackeray, M. M.; Rossouw, M. H.; de Kock, A.; de la Harpe, A. P.; Gumrow, R. J.; Pearce, K.; Liles, D. C. The versatility of MnO_2 for lithium battery applications. *J. Power Sources* **1993**, *43*, 289–300.
- (7) Johnson, C.; Kim, J.; Lefief, C.; Li, N.; Vaughey, J.; Thackeray, M. The significance of the Li_2MnO_3 component in ‘composite’ $x\text{Li}_2\text{MnO}_3\cdot(1-x)\text{LiMn}_{0.5}\text{Ni}_{0.5}\text{O}_2$ electrodes. *Electrochim. Commun.* **2004**, *6*, 1085.
- (8) Thackeray, M. M.; Johnson, C. S.; Vaughey, J. T.; Li, N.; Hackney, S. A. Advances in manganese-oxide ‘composite’ electrodes for lithium-ion batteries. *J. Mater. Chem.* **2005**, *15*, 2257.
- (9) Thackeray, M. M.; Kang, S.-H.; Johnson, C.; Vaughey, J.; Hackney, S. Comments on the structural complexity of lithium-rich $\text{Li}_{1+x}\text{M}_{1-x}\text{O}_2$ electrodes ($M = \text{Mn, Ni, Co}$) for lithium batteries. *Electrochim. Commun.* **2006**, *8*, 1531.
- (10) Thackeray, M. M.; Kang, S.-H.; Johnson, C. S.; Vaughey, J. T.; Benedek, R.; Hackney, S. Li_2MnO_3 -stabilized LiMO_2 ($M = \text{Mn, Ni, Co}$) electrodes for lithium-ion batteries. *J. Mater. Chem.* **2007**, *17*, 3112–3125.
- (11) Rossen, E.; Jones, C.; Dahn, J. Structure and electrochemistry of $\text{Li}_x\text{Mn}_{1-y}\text{O}_2$. *Solid State Ionics* **1992**, *57*, 311.
- (12) Lu, Z.; MacNeil, D.; Dahn, J. Layered cathode materials $\text{Li}[\text{Ni}_x\text{Li}_{(1/3-2x/3)}\text{Mn}_{(2/3-x/3)}]\text{O}_2$ for lithium-ion batteries. *Electrochim. Solid-State Lett.* **2001**, *4*, A191.
- (13) Lu, Z.; Beaulieu, L.; Donaberger, R.; Thomas, C.; Dahn, J. Synthesis, Structure, and Electrochemical Behavior of $\text{Li}[\text{Ni}_x\text{Li}_{(1/3-2x/3)}\text{Mn}_{(2/3-x/3)}]\text{O}_2$. *J. Electrochim. Soc.* **2002**, *149*, A778.
- (14) Lu, Z.; Dahn, J. R. Understanding the anomalous capacity of $\text{Li}/\text{Li}[\text{Ni}_x\text{Li}_{(1/3-2x/3)}\text{Mn}_{(2/3-x/3)}]\text{O}_2$ cells using in situ X-ray diffraction and electrochemical studies. *J. Electrochim. Soc.* **2002**, *149*, A815.
- (15) Dunn, B.; Kamath, H.; Tarascon, J.-M. Electrical energy storage for the grid: a battery of choices. *Science* **2011**, *334*, 928.

- (16) Rozier, P.; Tarascon, J. M. Li-rich layered oxide cathodes for next-generation Li-ion batteries: chances and challenges. *J. Electrochem. Soc.* **2015**, *162*, A2490.
- (17) Jarvis, K. A.; Deng, Z.; Allard, L. F.; Manthiram, A.; Ferreira, P. J. Atomic structure of a lithium-rich layered oxide material for lithium-ion batteries: evidence of a solid solution. *Chemistry of materials* **2011**, *23*, 3614.
- (18) Shukla, A. K.; Ramasse, Q. M.; Ophus, C.; Duncan, H.; Hage, F.; Chen, G. Unravelling structural ambiguities in lithium-and manganese-rich transition metal oxides. *Nat. Commun.* **2015**, *6*, 8711.
- (19) Yu, H.; Ishikawa, R.; So, Y. G.; Shibata, N.; Kudo, T.; Zhou, H.; Ikuhara, Y. Direct Atomic Resolution Observation of Two Phases in the $\text{Li}_{1.2}\text{Mn}_{0.567}\text{Ni}_{0.166}\text{Co}_{0.067}\text{O}_2$ Cathode Material for Lithium Ion Batteries. *Angew. Chem., Int. Ed.* **2013**, *52*, 5969.
- (20) Kang, S.-H.; Kempgens, P.; Greenbaum, S.; Kropf, A.; Amine, K.; Thackeray, M. Interpreting the structural and electrochemical complexity of $0.5\text{Li}_2\text{MnO}_3\text{-}0.5\text{LiMO}_2$ electrodes for lithium batteries ($M=\text{Mn}_{0.5-x}\text{Ni}_{0.5-x}\text{Co}_{2x}, 0 \leq x \leq 0.5$). *J. Mater. Chem.* **2007**, *17*, 2069.
- (21) Seo, D.-H.; Lee, J.; Urban, A.; Malik, R.; Kang, S.; Ceder, G. The structural and chemical origin of the oxygen redox activity in layered and cation-disordered Li-excess cathode materials. *Nature Chem.* **2016**, *8*, 692.
- (22) Luo, K.; Roberts, M. R.; Hao, R.; Guerrini, N.; Pickup, D. M.; Liu, Y.-S.; Edstrom, K.; Guo, J.; Chadwick, A. V.; Duda, L. C.; Bruce, P. G. Charge-compensation in 3d-transition-metal-oxide intercalation cathodes through the generation of localized electron holes on oxygen. *Nature Chem.* **2016**, *8*, 684.
- (23) McCalla, E.; Abakumov, A. M.; Saubanère, M.; Foix, Berg, E. J.; Rousse, G.; Doublet, M. L.; Gonbeau, D.; Novák, P.; Van Tendeloo, G.; Dominko, R.; Tarascon, J.-M. Visualization of OO peroxy-like dimers in high-capacity layered oxides for Li-ion batteries. *Science* **2015**, *350*, 1516.
- (24) Sathiya, M.; Rousse, G.; Ramesha, K.; Laisa, C. P.; Vezin, H.; Sougrati, M. T.; Doublet, M.-L.; Foix, D.; Gonbeau, D.; Walker, W.; Prakash, A.; et al. S.; Ben Hassine, M.; Dupont, L.; and Tarascon, J.-M. Reversible anionic redox chemistry in high-capacity layered-oxide electrodes. *Nature materials* **2013**, *12*, 827.
- (25) Qiu, B.; Zhang, M.; Xia, Y.; Liu, Z.; Meng, Y. S. Understanding and controlling anionic electrochemical activity in high-capacity oxides for next generation Li-ion batteries. *Chem. Mater.* **2017**, *29*, 908.
- (26) van Bommel, A.; Dahn, J. Kinetics study of the high potential range of lithium-rich transition-metal oxides for lithium-ion batteries by electrochemical methods. *Electrochim. Solid-State Lett.* **2010**, *13*, A62.
- (27) Yu, H.; Wang, Y.; Asakura, D.; Hosono, E.; Zhang, T.; Zhou, H. Electrochemical kinetics of the $0.5\text{Li}_2\text{MnO}_{3.0.5}\text{LiMn}_{0.42}\text{Ni}_{0.42}\text{Co}_{0.16}\text{O}_2$ 'composite' layered cathode material for lithium-ion batteries. *Rsc Advances* **2012**, *2*, 8797.
- (28) Kang, S.-H.; Thackeray, M. M. Enhancing the rate capability of high capacity $x\text{Li}_2\text{MnO}_3\text{-}(1-x)\text{LiMO}_2$ ($M=\text{Mn, Ni, Co}$) electrodes by LiNiPO_4 treatment. *Electrochim. Commun.* **2009**, *11*, 748.
- (29) Croy, J. R.; Kim, D.; Balasubramanian, M.; Gallagher, K.; Kang, S.-H.; Thackeray, M. M. Counteracting the Voltage Decay in High Capacity $x\text{Li}_2\text{MnO}_3\bullet(1-x)\text{LiMO}_2$ Electrodes ($M=\text{Mn, Ni, Co}$) for Li^+ -Ion Batteries. *J. Electrochim. Soc.* **2012**, *159*, A781–790.
- (30) Croy, J. R.; Balasubramanian, M.; Gallagher, K. G.; Burrell, A. K. Review of the US Department of Energy's "deep dive" effort to understand voltage fade in Li-and Mn-rich cathodes. *Accounts of chemical research* **2015**, *48*, 2813.
- (31) Mohanty, D.; Kalnaus, S.; Meisner, R. A.; Rhodes, K. J.; Li, J.; Payzant, E. A.; Wood, D. L.; Daniel, C. Structural transformation of a lithium-rich $\text{Li}_{1.2}\text{Co}_{0.1}\text{Mn}_{0.55}\text{Ni}_{0.15}\text{O}_2$ cathode during high voltage cycling resolved by in situ X-ray diffraction. *J. Power Sources* **2013**, *229*, 239.
- (32) Meng, Y.; Ceder, G.; Grey, C.; Yoon, W.-S.; Jiang, M.; Breger, J.; Shao-Horn, Y. Cation Ordering in Layered O_3 $\text{Li}_{[N_x\text{Li}_{1/3-2x/3}\text{Mn}_{2/3-x/3}]}\text{O}_2$ ($0 \leq x \leq 1/2$) Compounds. *Chem. Mater.* **2005**, *17*, 2386.
- (33) Lei, C.; Barenco, J.; Wen, J.; Petrov, I.; Kang, S.-H.; Abraham, D. Local structure and composition studies of $\text{Li}_{1.2}\text{Ni}_{0.2}\text{Mn}_{0.6}\text{O}_2$ by analytical electron microscopy. *J. Power Sources* **2008**, *178*, 422.
- (34) Boulineau, A.; Croguennec, L.; Delmas, C.; Weill, F. Reinvestigation of Li_2MnO_3 Structure: Electron Diffraction and High Resolution TEM. *Chem. Mater.* **2009**, *21*, 4216.
- (35) Yu, H.; Zhou, H. High-Energy Cathode Materials ($\text{Li}_2\text{MnO}_3\text{-LiMO}_2$) for Lithium-Ion Batteries. *Journal of physical chemistry letters* **2013**, *4*, 1268.
- (36) McCalla, E.; Rowe, A.; Brown, C.; Hacquebard, L.; Dahn, J. How phase transformations during cooling affect Li-Mn-Ni-O positive electrodes in lithium ion batteries. *J. Electrochim. Soc.* **2013**, *160*, A1134.
- (37) Li, J.; Camardese, J.; Glazier, S.; Dahn, J. Structural and electrochemical study of the Li-Mn-Ni oxide system within the layered single phase region. *Chem. Mater.* **2014**, *26*, 7059.
- (38) Jarvis, K. A.; Wang, C.-C.; Manthiram, A.; Ferreira, P. J. The role of composition in the atomic structure, oxygen loss, and capacity of layered Li-Mn-Ni oxide cathodes. *Journal of Materials Chemistry A* **2014**, *2*, 1353.
- (39) Genevois, C. C.; Koga, H.; Croguennec, L.; Ménétrier, M.; Delmas, C.; Weill, F. Insight into the Atomic Structure of Cycled Lithium-Rich Layered Oxide $\text{Li}_{1.20}\text{Mn}_{0.54}\text{Co}_{0.13}\text{Ni}_{0.13}\text{O}_2$ Using HAADF STEM and Electron Nanodiffraction. *J. Phys. Chem. C* **2015**, *119*, 75.
- (40) Ruther, R. E.; Callender, A. F.; Zhou, H.; Martha, S. K.; Nanda, J. Raman microscopy of lithium-manganese-rich transition metal oxide cathodes. *J. Electrochim. Soc.* **2015**, *162*, A98.
- (41) Yan, P.; Zheng, J.; Lv, D.; Wei, Y.; Zheng, J.; et al. Atomic-resolution visualization of distinctive chemical mixing behavior of Ni, Co, and Mn with Li in layered lithium transition-metal oxide cathode materials. *Chem. Mater.* **2015**, *27*, 5393.
- (42) Armstrong, A. R.; Holzapfel, M.; Novák, P.; Johnson, C. S.; Kang, S.-H.; Thackeray, M. M.; Bruce, P. G. Demonstrating Oxygen Loss and Associated Structural Reorganization in the Lithium Battery Cathode $\text{Li}[\text{Ni}_{0.2}\text{Li}_{0.2}\text{Mn}_{0.6}]_{\text{O}_2}$. *J. Am. Chem. Soc.* **2006**, *128*, 8694.
- (43) Johnson, C. S.; Li, N.; Lefief, C.; Vaughney, J. T.; Thackeray, M. M. Synthesis, Characterization and Electrochemistry of Lithium Battery Electrodes: $x\text{Li}_2\text{MnO}_3\text{-}(1-x)\text{LiMn}_{0.333}\text{Ni}_{0.333}\text{Co}_{0.333}\text{O}_2$ ($0 \leq x \leq 0.7$). *Chem. Mater.* **2008**, *20*, 6095–6106.
- (44) Kim, D.; Gim, J.; Lim, J.; Park, S.; Kim, J. Synthesis of $x\text{Li}_2\text{MnO}_3\text{-}(1-x)\text{LiMO}_2$ ($M=\text{Cr, Mn, Co, Ni}$) nanocomposites and their electrochemical properties. *Mater. Res. Bull.* **2010**, *45*, 252.
- (45) Barenco, J.; Lei, C.; Wen, J.; Kang, S. H.; Petrov, I.; Abraham, D. Local Structure of Layered Oxide Electrode Materials for Lithium-Ion Batteries. *Advanced materials* **2010**, *22*, 1122.
- (46) Barenco, J.; Balasubramanian, M.; Kang, S.; Wen, J.; Lei, C.; Pol, S.; Petrov, I.; Abraham, D. Long-Range and Local Structure in the Layered Oxide $\text{Li}_{1.2}\text{Co}_{0.4}\text{Mn}_{0.4}\text{O}_2$. *Chem. Mater.* **2011**, *23*, 2039.
- (47) Wen, J.; Barenco, J.; Lei, C.; Kang, S.; Balasubramanian, M.; Petrov, I.; Abraham, D. Analytical electron microscopy of $\text{Li}_{1.2}\text{Co}_{0.4}\text{Mn}_{0.4}\text{O}_2$ for lithium-ion batteries. *Solid State Ionics* **2011**, *182*, 98.
- (48) Gu, M.; Belharouak, I.; Genc, A.; Wang, Z.; Wang, D.; Amine, K.; Gao, F.; Zhou, G.; Thevuthasan, S.; Baer, D. R.; Zhang, J.-G.; Browning, N. D.; Liu, J.; Wang, C. Conflicting Roles of Nickel in Controlling Cathode Performance in Lithium Ion Batteries. *Nano Lett.* **2012**, *12*, S186–5191.
- (49) Boulineau, A.; Simonin, L.; Colin, J.-F.; Canévet, E.; Daniel, L.; Patoux, S. B. Evolutions of $\text{Li}_{1.2}\text{Mn}_{0.61}\text{Ni}_{0.18}\text{Mg}_{0.01}\text{O}_2$ during the Initial Charge/Discharge Cycle Studied by Advanced Electron Microscopy. *Chem. Mater.* **2012**, *24*, 3558.
- (50) Gu, M.; Belharouak, I.; Zheng, J.; Wu, H.; Xiao, J.; Genc, A.; Amine, K.; Thevuthasan, S.; Baer, D. R.; Zhang, J.-G.; Browning, N. D.; Liu, J.; Wang, C. Formation of the Spinel Phase in the Layered Composite Cathode Used in Li-Ion Batteries. *ACS Nano* **2013**, *7*, 760–767.
- (51) Yu, H.; Kim, H.; Wang, Y.; He, P.; Asakura, D.; Nakamura, Y.; Zhou, H. High-energy 'composite' layered manganese-rich cathode materials via controlling Li_2MnO_3 phase activation for lithium-ion batteries. *Phys. Chem. Chem. Phys.* **2012**, *14*, 6584.

- (52) Mohanty, D.; Huq, A.; Payzant, E. A.; Sefat, A. S.; Li, J.; Abraham, D. P.; Wood, D. L.; Daniel, C. Neutron Diffraction and Magnetic Susceptibility Studies on a High-Voltage $\text{Li}_{1.2}\text{Mn}_{0.55}\text{Ni}_{0.15}\text{Co}_{0.10}\text{O}_2$ Lithium Ion Battery Cathode: Insight into the Crystal Structure. *Chem. Mater.* **2013**, *25*, 4064.
- (53) Rana, J.; Kloepsch, R.; Li, J.; Scherb, T.; Schumacher, G.; Winter, M.; Banhart, J. On the structural integrity and electrochemical activity of a $0.5\text{Li}_2\text{MnO}_3\text{-}0.5\text{LiCoO}_2$ cathode material for lithium-ion batteries. *Journal of Materials Chemistry A* **2014**, *2*, 9099.
- (54) Ammundsen, B.; Paulsen, J.; Davidson, I.; Liu, R.-S.; Shen, C.-H.; Chen, J.-M.; Jang, L.-Y.; Lee, J.-F. Local structure and first cycle redox mechanism of layered $\text{Li}_{1.2}\text{Cr}_{0.4}\text{Mn}_{0.4}\text{O}_2$ Cathode Material. *J. Electrochem. Soc.* **2002**, *149*, A431.
- (55) Lu, Z.; Chen, Z.; Dahn, J. Lack of Cation Clustering in $\text{Li}[\text{Ni}_x\text{Li}_{1/3-2x/3}\text{Mn}_{2/3-x/3}] \text{O}_2$ ($0 < x \leq 1/2$) and $\text{Li}[\text{Cr}_x\text{Li}_{(1-x)/3}\text{Mn}_{(2-2x)/3}] \text{O}_2$ ($0 < x < 1$). *Chem. Mater.* **2003**, *15*, 3214–3220.
- (56) Koga, H.; Croguennec, L.; Mannessiez, P.; Ménétrier, M.; Weill, F. O.; Bourgeois, L.; Duttine, M.; Suard, E.; Delmas, C. and Delmas, C. $\text{Li}_{1.20}\text{Mn}_{0.54}\text{Co}_{0.13}\text{Ni}_{0.13}\text{O}_2$ with Different Particle Sizes as Attractive Positive Electrode Materials for Lithium-Ion Batteries: Insights into Their Structure. *J. Phys. Chem. C* **2012**, *116*, 13497.
- (57) Bréger, J.; Jiang, M.; Dupré, N.; Meng, Y. S.; Shao-Horn, Y.; Ceder, G.; Grey, C. P. High-resolution X-ray diffraction, DIFFaX, NMR and first principles study of disorder in the $\text{Li}_2\text{MnO}_3\text{-Li}[\text{Ni}_{1/2}\text{Mn}_{1/2}] \text{O}_2$ solid solution. *J. Solid State Chem.* **2005**, *178*, 2575.
- (58) Ohzuku, T.; Nagayama, M.; Tsuji, K.; Ariyoshi, K. High-capacity lithium insertion materials of lithium nickel manganese oxides for advanced lithium-ion batteries: toward rechargeable capacity more than 300 mAh g^{-1} . *J. Mater. Chem.* **2011**, *21*, 10179.
- (59) Jarvis, K.; Deng, Z.; Manthiram, A.; Ferreira, P. Understanding the role of lithium content on the structure and capacity of lithium-rich layered oxides by aberration-corrected STEM, D-STEM, and EDS. *Microscopy and Microanalysis* **2012**, *18*, 1484.
- (60) Rowe, A.; Camardese, J.; McCalla, E.; Dahn, J. High Precision Coulometry Studies of Single-Phase Layered Compositions in the Li-Mn-Ni-O System. *J. Electrochem. Soc.* **2014**, *161*, A1189–1193.
- (61) Johnston-Peck, A. C.; Levin, I.; Herzing, A. A.; Bendersky, L. A. Structural studies of $\text{Li}_{1.2}\text{Mn}_{0.55}\text{Ni}_{0.15}\text{Co}_{0.1}\text{O}_2$ electrode material. *Mater. Charact.* **2016**, *119*, 120.
- (62) Zunger, A.; Wei, S.-H.; Ferreira, L.; Bernard, J. E. Special quasirandom structures. *Phys. Rev. Lett.* **1990**, *65*, 353.
- (63) van de Walle, A.; Tiwary, P.; de Jong, M.; Olmsted, D. L.; Asta, M.; Dick, A.; Shin, D.; Wang, Y.; Chen, L.-Q.; Liu, Z.-K. Efficient stochastic generation of special quasirandom structures. *Calphad* **2013**, *42*, 13.
- (64) Doak, J. W.; Wolverton, C. Coherent and incoherent phase stabilities of thermoelectric rocksalt IV-VI semiconductor alloys. *Phys. Rev. B* **2012**, *86*, 144202.
- (65) Wolverton, C.; Zunger, A. Cation and vacancy ordering in Li_xCoO_2 . *Phys. Rev. B* **1998**, *57*, 2242.
- (66) Wolverton, C.; Zunger, A. Prediction of Li Intercalation and Battery Voltages in Layered vs. Cubic Li_xCoO_2 . *J. Electrochem. Soc.* **1998**, *145*, 2424.
- (67) Lee, S.; Park, S. S. Atomistic Simulation Study of Mixed-Metal Oxide ($\text{LiNi}_{1/3}\text{Co}_{1/3}\text{Mn}_{1/3}\text{O}_2$) Cathode Material for Lithium Ion Battery. *J. Phys. Chem. C* **2012**, *116*, 6484.
- (68) Luo, G.; Zhao, J.; Ke, X.; Zhang, P.; Sun, H.; Wang, B. Structure, electrode voltage and activation energy of $\text{LiMn}_x\text{Co}_y\text{Ni}_{1-x-y}\text{O}_2$ solid solutions as cathode materials for Li batteries from first-principles. *J. Electrochem. Soc.* **2012**, *159*, A1203.
- (69) Koyama, Y.; Tanaka, I.; Nagao, M.; Kanno, R. First-principles study on lithium removal from Li_2MnO_3 . *J. Power Sources* **2009**, *189*, 798.
- (70) Okamoto, Y. Ambivalent effect of oxygen vacancies on Li_2MnO_3 : a first-principles study. *J. Electrochem. Soc.* **2011**, *159*, A152.
- (71) Xiao, R.; Li, H.; Chen, L. Density Functional Investigation on Li_2MnO_3 . *Chem. Mater.* **2012**, *24*, 4242.
- (72) Koyama, Y.; Arai, H.; Tanaka, I.; Uchimoto, Y.; Ogumi, Z. Defect Chemistry in Layered LiMO_2 ($\text{M} = \text{Co}, \text{Ni}, \text{Mn}$, and $\text{Li}_{1/3}\text{Mn}_{2/3}$) by First-Principles Calculations. *Chem. Mater.* **2012**, *24*, 3886.
- (73) Lee, E.; Persson, K. A. Structural and Chemical Evolution of the Layered Li-Excess Li_xMnO_3 as a Function of Li Content from First-Principles Calculations. *Adv. Energy Mater.* **2014**, *4*, 1400498.
- (74) Xu, B.; Fell, C. R.; Chi, M.; Meng, Y. S. Identifying surface structural changes in layered Li-excess nickel manganese oxides in high voltage lithium ion batteries: A joint experimental and theoretical study. *Energy Environ. Sci.* **2011**, *4*, 2223.
- (75) Iddir, H.; Benedek, R. First-principles analysis of phase stability in layered-layered composite cathodes for lithium-ion batteries. *Chem. Mater.* **2014**, *26*, 2407.
- (76) Hardy, H. A “sub-regular” solution model and its application to some binary alloy systems. *Acta Metall.* **1953**, *1*, 202.
- (77) Wolverton, C.; Ozolins, V.; Zunger, A. Short-range-order types in binary alloys: a reflection of coherent phase stability. *J. Phys.: Condens. Matter* **2000**, *12*, 2749.